

An Investigation into the Stability Characteristics of a Tilt-Rotor Configuration in Turning Flight using Advanced Modelling and Fast Analysis Techniques

J. Scott G. McVicar*

Roy Bradley†

Department of Mathematics,
Glasgow Caledonian University,
Glasgow,
G4 0BA

Abstract

This paper will present innovative techniques for use in the trimming and stability analysis of advanced models of rotorcraft. It begins by exploiting the rotor symmetry to produce an efficient definition of periodic trim which is applicable to rotorcraft simulations. This definition is then used as the basis of a trimming algorithm which is capable of trimming advanced simulation models to a specified periodic trim state. The definition of periodic trim is then used to derive a technique for use in the stability analysis of advanced simulations. This technique is a specialised enhancement of classical Floquet theory and exploits the rotor symmetry to reduce computational burden. The trim and stability analysis techniques are then used, in conjunction with an individual blade simulation model, to assess the stability characteristics of the XV-15 tilt-rotor whilst it is performing a banked turn. This study demonstrates that the trimming algorithm is efficient and robust to the quality of its start values and that the stability analysis is capable of identifying accurately all the modes of the non-linear model.

1 Nomenclature

A, \bar{A}	System matrix, averaged system matrix
A_{flap}	Partition of system matrix containing the flap derivatives
c	Control state vector
J	Jacobian matrix
m	Number of model states
n	Number of blades per rotor
$nsteps$	Number of time steps in a complete revolution of rotor azimuth
p, q, r	Fuselage roll, pitch and yaw rates about body axis set
P_v, P_r	Vehicle overall permutation matrix, rotor permutation matrix
P_6	Permutation matrix for a 3 bladed rotor with two flapping states per blade
R	Floquet Transition matrix
S	Partial Floquet Transition matrix
sc	Vector of initial body states and control states
$s_{fs}, s_{if}, s_{rr}(t)$	Body axis, induced flow and right (left) rotor state vectors
s_v	Vehicle state vector
s_x	Vector comprising vehicle states at $2\pi/n$ and mean flight path states
$t_{0.5}$	Time to half amplitude
t_p	Time for one period of oscillation in rotor forces and moments
T	Time for one full revolution of rotor azimuth
u_a, v_a, w_a	Fuselage velocity components along x, y and z body axis respectively

*Research Fellow

†Professor

$v_{0r(l)}$	Uniform induced flow component for right (left) rotor
$v_{1sr(l)}, v_{1cr(l)}$	Harmonic induced flow components for right (left) rotor
V	Magnitude of vehicle speed
$\mathbf{x}, \bar{\mathbf{x}}, \mathbf{x}_{trim}$	Flight state vector, mean flight state vector and specified mean flight state vector
β	Blade flapping angle, fuselage sideslip angle
$\beta_0, \beta_{1c}, \beta_{1s}$	Harmonics of blade flap
ϵ	Error vector
γ, θ, ϕ	Fuselage angles of climb, pitch and roll
γ_n	nacelle incidence (measured from helicopter mode)
λ, Λ	Continuous eigenvalue, discrete eigenvalue
θ_{0c}, θ_{0d}	Combined and differential collective inputs
$\theta_{1sc}, \theta_{1sd}$	Combined and differential longitudinal cyclic inputs
θ_{1cc}	Combined lateral cyclic
σ, ω	Real and imaginary parts of continuous eigenvalue
Ω	Fuselage turn rate
Ω_r	Rotor Speed
ψ_r	Rotor azimuth angle

2 Introduction

Future rotorcraft will be required to perform manoeuvres across a broad flight envelope in order to attain high levels of agility and realize a wide range of applications [1]. When performing such manoeuvres, non-linear aerodynamics and higher order rotor dynamics will exert a significant influence on the flying characteristics of the vehicle. Previous generation, or Level 1 [2], simulations sacrifice fidelity by neglecting these effects and therefore Level 1 models are inappropriate for a complete assessment of rotorcraft handling qualities throughout the vehicle's operating environment. A new generation of simulations (or Level 2 simulations) has been developed to support design studies across a larger extent of the flight envelope. These models attain the necessary levels of fidelity by incorporating individual blade modelling techniques in conjunction with numerical integration of the rotor loads and non-linear aerodynamics; features such as compressibility and blade elasticity are also often included. Before the potential offered by Level 2 simulations may be fully exploited, new analysis techniques must be developed so that the high levels of fidelity are accessible to the flight dynamicist and control system engineer. This paper will focus on two such key areas, namely, the determination of rotorcraft trim conditions and evaluation of stability characteristics from Level 2 simulations.

Generally, the evaluation of a specified trim state represents the starting point for any simulation, consequently, it is vitally important that the associated trim algorithm is both robust and efficient. Level 2 simulations adopt trim conditions, achieved with constant control positions, which are no longer time invariant (as is the case with Level 1 simulations) but are periodic about a fixed mean. Therefore, when seeking a trim condition, it is necessary to obtain a periodic solution to the equations of motion which satisfies the stipulated flight condition in the mean. This paper will begin by presenting a modified periodic shooting algorithm which is capable of reliably and efficiently trimming Level 2 rotorcraft simulations.

The operation of rotorcraft in adverse areas of the flight envelope promotes the requirement for control systems of increasing complexity in order to preserve acceptable handling qualities throughout the operational environment. This fact is recognised by the authors of the U.S. Handling Qualities for Military Rotorcraft [3] who make recommendations on the development of new high bandwidth control systems for application to rotorcraft. It is generally accepted that the integrity of these high bandwidth control systems will be largely dependent on a detailed knowledge of the vehicle higher order dynamics and in particular the rotor and structural modes will be of increasing significance [1]. Level 2 simulations encompass the higher order dynamics of the vehicle and are therefore ideally suited to support the design of high bandwidth control systems. However, fast and reliable stability analysis techniques are essential if these models are to yield practical benefit in the formulation of control laws. This paper will derive a specialised technique for assessing rotorcraft stability characteristics from Level 2 simulations. The technique is essentially an extension of classical Floquet theory and exploits the symmetry of the rotor to produce an efficient approach which is specific to Level 2 simulations.

The trim and stability analysis algorithms developed in this paper have been extensively applied to an individual blade simulation (TILTSTAB) of a generic tilt-rotor configuration [4]. The paper will proceed by presenting results obtained when trim and stability analysis are performed on a tilt-rotor vehicle which is performing a banked turn in transition mode. This section of the paper will demonstrate that the trimming

algorithm is robust to the quality of initial values and capable of rapidly producing very high quality trim states. The results presented from the stability analysis will show that this technique is capable of identifying both the rigid body and higher order rotor modes of the full non-linear simulation model. Furthermore, these results will highlight limitations in the widely adopted *Average A* stability analysis technique [5] when identifying the higher order rotor modes.

From the preceding discussions it should be apparent that the periodic trim state adopted by Level 2 simulations is central to the trim and stability analysis algorithms derived in this paper. The most appropriate introduction to these algorithms is therefore to develop a formal definition of the periodic trim state.

3 Partial Periodicity of Rotorcraft Trim States

The periodicity of rotorcraft trim states is a direct consequence of two factors influencing the behaviour of a rotor blade as it advances round the azimuth. Firstly, if a constant cyclic pitch input is applied, then the blade angle of attack will vary periodically as it advances round the azimuth. Secondly, if the vehicle has a non-zero velocity then the blade will experience a periodic variation in dynamic pressure as it rotates round the disc. Both these effects lead to a periodic solution of the trimmed rotor equations which in turn introduces periodicity in to all the trimmed model states. The model states naturally fall into three distinct categories reflecting the physical components of the vehicle:-

1. blade states
2. body axis flight states
3. induced flow states

and the periodic behaviour adopted by each of these components will now be considered in turn.

3.1 Periodicity of Trimmed Blade States

In the trim, each blade experiences once-per-revolution periodic forcing it travels round the rotor azimuth. Therefore, the full period of the trimmed blade states is described in one complete revolution of rotor azimuth. It is apparent that the period of the blade states is independent of the number of blades in the rotor. Thus, in the trim, for an n bladed model incorporating two flap states per blade:-

$$\mathbf{s}_r(2\pi) = \mathbf{s}_r(0) \quad (1)$$

where, in this case, the rotor state vector is given by:-

$$\mathbf{s}_r = \left[\beta_1 \quad \dot{\beta}_1 \quad \beta_2 \quad \dot{\beta}_2 \quad \vdots \quad \beta_n \quad \dot{\beta}_n \right]^T$$

The expression given in Equation 1 is a valid definition of a rotor in trim which relies on a complete revolution of rotor azimuth. A more economic definition can be obtained by considering the symmetry of the rotor when it consists solely of identical blades. In this situation, all blades trace out exactly the same trajectory as they advance round the rotor azimuth with a phase shift of $2\pi/n$ radians between the path of each successive blade. Thus, for a rotor in trim, the states of an arbitrary blade, m , at $\psi_r = 2\pi/n$ radians will map onto the initial states of the identical blade $m + 1$ when $\psi_r = 0$. This characteristic can be exploited to form a definition for a rotor in trim using only $2\pi/n$ radians of rotor revolution and may be expressed as:-

$$\mathbf{s}_r(2\pi/n) = P_r \mathbf{s}_r(0) \quad (2)$$

where the general form of the rotor permutation matrix, P_r , is given by:-

$$P_r = \begin{bmatrix} 0 & 0 & 1 & 0 & 0 & 0 & \dots & \dots & 0 & 0 \\ 0 & 0 & 0 & 1 & 0 & 0 & \dots & \dots & 0 & 0 \\ 0 & 0 & 0 & 0 & 1 & 0 & \dots & \dots & 0 & 0 \\ 0 & 0 & 0 & 0 & 0 & 1 & \dots & \dots & 0 & 0 \\ \vdots & \vdots & \vdots & \vdots & \vdots & \vdots & \dots & \dots & \vdots & \vdots \\ \vdots & \vdots & \vdots & \vdots & \vdots & \vdots & \dots & \dots & \vdots & \vdots \\ 0 & 0 & 0 & 0 & 0 & 0 & \dots & \dots & 1 & 0 \\ 0 & 0 & 0 & 0 & 0 & 0 & \dots & \dots & 0 & 1 \\ 1 & 0 & 0 & 0 & 0 & 0 & \dots & \dots & 0 & 0 \\ 0 & 1 & 0 & 0 & 0 & 0 & \dots & \dots & 0 & 0 \end{bmatrix}$$

As can be seen, the permutation matrix, P_r , takes the form of the identity matrix with the non-zero elements shifted to the right by an amount corresponding to the number of states per blade. The versatility of this definition is reflected by the ease in which more sophisticated rotor models can be accommodated. In particular, rotor models with more states per blade (e.g. lag or elastic states) can be included in this definition by shifting the non-zero permutation elements further to the right by an appropriate amount.

3.2 Periodicity of Trimmed Body Axis Flight States

The periodic nature of the trimmed body axis flight states is strongly dependent on the characteristics of the rotor forces and moments which drive the equations of motion. In the trim, any given azimuthal location round the rotor disc will have its own associated blade pitch and aerodynamic velocity and thus, for a rotor with identical blades, each blade will generate exactly the same contribution to the rotor forces and moments as it passes through that azimuthal location. An n bladed rotor must rotate through $2\pi/n$ radians to have had, instantaneously, a blade in all azimuthal locations and therefore the full period of the rotor forces and moments is described in $2\pi/n$ radians of revolution. As a result, the vehicle body states will also adopt a periodic trajectory in the trim and the full period of this trajectory will be given in $2\pi/n$ radians of rotor azimuth. When a trimmed flight state has been achieved, the vehicle body states satisfy:-

$$\mathbf{s}_{fs}(2\pi/n) = \mathbf{s}_{fs}(0) \quad (3)$$

where the body axis flight state vector is given by:-

$$\mathbf{s}_{fs} = [u_a \quad v_a \quad w_a \quad p \quad q \quad r \quad \theta \quad \phi]^T.$$

3.3 Periodicity of Trimmed Induced Flow States

Direct inclusion of the rotor induced states into the definition of periodic trim is dependent on the induced flow model being used. When induced flow models of the Glauert [6] type are included, the initial induced flow states corresponding to a set of trimmed initial rotor and body states can be ascertained iteratively without direct inclusion in the trim algorithm. Dynamic inflow models [7] typically incorporate a first order differential equation to model the rotor induced flow field. Consequently, it is necessary to ascertain the trimmed initial states of this equation by direct inclusion in the trimming algorithm. The induced flow field generated by the rotor is driven directly by the thrust and aerodynamic moments and therefore, the periodicity of the trimmed induced flow states will be described in $2\pi/n$ radians of rotor revolution. If the rotor is in trim the induced flow states satisfy:-

$$\mathbf{s}_{if}(2\pi/n) = \mathbf{s}_{if}(0) \quad (4)$$

for a tilt-rotor, the induced flow state vector (containing a uniform component and two harmonics for each rotor) is given by:-

$$\mathbf{s}_{if} = [v_{0r} \quad v_{1sr} \quad v_{1cr} \quad v_{0t} \quad v_{1cr} \quad v_{1cl}]^T.$$

3.4 Definition of Vehicle Trim

The expressions given in Equations 2, 3, 4 can be combined to define the overall vehicle trim. For a simulation with two three bladed rotors, two flapping states per blade and three inflow states per rotor the overall definition of trim becomes:-

$$\mathbf{s}_v(2\pi/n) = P_v \mathbf{s}_v(0). \quad (5)$$

Where, in this case $n=3$, and the vehicle permutation matrix, P_v , is given by:-

$$P_v = \begin{bmatrix} P_6 & 0 & 0 & 0 \\ 0 & P_6 & 0 & 0 \\ 0 & 0 & I_6 & 0 \\ 0 & 0 & 0 & I_8 \end{bmatrix}.$$

The vehicle state vector is given by:-

$$\mathbf{s}_v = [\mathbf{s}_{rr} \quad \mathbf{s}_{lr} \quad \mathbf{s}_{if} \quad \mathbf{s}_{fs}]^T.$$

The definition of rotorcraft trim given by Equation 5 is central to the derivation of the economical trim and stability analysis algorithms which are described in the following sections of this paper.

4 Partial Periodic Trim Algorithm

Two problems require solution when seeking a given specified periodic trim state. Firstly, one must ascertain the correct set of initial conditions to ensure periodicity in the flight state (i.e., satisfy Equation 5). Secondly, one must obtain the set of control displacements necessary to produce the specified trim state.

For Level 2 simulations, the trimmed flight path is most conveniently specified in terms of the time averaged integral across one period of the flight path states [4, 8]:-

$$\bar{\mathbf{x}} = \frac{1}{t_p} \int_0^{t_p} \mathbf{x} dt \quad (6)$$

When considering the tilt-rotor application, five control states are available to the pilot:-

$$\mathbf{c} = [\theta_{0c} \quad \theta_{0d} \quad \theta_{1sc} \quad \theta_{1sd} \quad \theta_{1cc}]^T$$

therefore, the flight path may be specified in terms of the following five parameters [4, 8]:-

$$\mathbf{x}_{\text{trim}} = [V \quad \beta \quad \gamma \quad \Omega \quad \phi]^T.$$

Once the required set of control displacements have been obtained, the time averaged integral given by Equation 6 will equal the specified trim state:-

$$\bar{\mathbf{x}} = \mathbf{x}_{\text{trim}}. \quad (7)$$

Together, Equations 5 and 7 define the conditions which must be satisfied to attain a given specified periodic trim state. The trimming process now reduces to an iterative procedure which yields the blend of initial conditions, $\mathbf{s}_v(0)$, and control displacements, \mathbf{c} , necessary to satisfy Equations 5 and 7. For this application, a linearisation derived from a Taylor expansion about the solution values results in the following Newton-Raphson iteration scheme with periodic shooting:-

$$\begin{bmatrix} \mathbf{s}_v(0) \\ \mathbf{c} \end{bmatrix}_{i+1} = \begin{bmatrix} \mathbf{s}_v(0) \\ \mathbf{c} \end{bmatrix}_i - \begin{bmatrix} J_{11} - P_v & J_{12} \\ J_{21} & J_{22} \end{bmatrix}^{-1} \begin{bmatrix} \mathbf{s}_v(2\pi/n) - P_v \mathbf{s}_v(0) \\ \bar{\mathbf{x}} - \mathbf{x}_{\text{trim}} \end{bmatrix} \quad (8)$$

where J_{11} , J_{12} , J_{13} and J_{22} are partitions of the Jacobian matrix, J . In this case, the elements of the Jacobian are given by:-

$$J_{ij} = \frac{\partial s_{x_i}}{\partial s_{c_j}}$$

and the vector, \mathbf{s}_x , comprises the vehicle states at $2\pi/n$ and mean flight path states:-

$$\mathbf{s}_x = \begin{bmatrix} \mathbf{s}_v(2\pi/n) \\ \bar{\mathbf{x}} \end{bmatrix} \quad (9)$$

and the vector of control and initial vehicle states, \mathbf{s}_c is given by:-

$$\mathbf{s}_c = \begin{bmatrix} \mathbf{s}_v(0) \\ \mathbf{c} \end{bmatrix}$$

We will term the iteration scheme given by Equation 8 as the Partial Periodic Trimming Algorithm (PPTA). This technique yields extremely high levels of computational efficiency in three ways:-

1. the definition of vehicle trim, given by Equation 5, is exploited during the periodic shooting phase in which the non-linear model is integrated through only $2\pi/n$ radians of rotor azimuth
2. the PPTA is a single stage method which obtains simultaneously the initial conditions, $\mathbf{s}_v(0)$, and control displacements, \mathbf{c} , to provide the specified periodic flight condition
3. the PPTA is particularly robust and there has been no recourse to damping or acceleration parameters to improve the stability characteristics of the iteration scheme.

The PPTA offers considerable advantages (in terms of both robustness and computational efficiency) over those iterative techniques which disregard the periodic property of the trim state and rely on integrating the equations of motion until the transients sufficiently decay. Such techniques have their performance dictated by the rate of decay of the most persistent natural mode. Since rotorcraft typically possess at least one lightly damped mode (and are often unstable), such methods are usually several orders of magnitude slower (if they converge at all) than those which exploit the periodicity of the equations. In order to enhance the performance of these slower schemes there is often recourse to techniques such as the freezing of body states or model order reduction. The implication of these approximations is that different models are used during the trimming and forward simulation phases. Consequently, the quality of the resulting trim state is compromised and transient behaviour is evident in the forward simulation. When using the PPTA, there is no requirement for simplification of the model structure in order to reduce computational times to an acceptable level. Therefore, exactly the same model is used during trimming and forward simulation phases. This results in exceptionally high quality trim states which are maintained for extended periods of forward simulation.

The efficiency of the PPTA and the quality of the trim states it produces will be demonstrated in the case study presented in Section 6 of this paper.

5 Stability Analysis of Level 2 Rotorcraft Simulations

The equations of motion for the full non-linear simulation model (controls fixed) may be written as an Initial Value Problem of order m :-

$$\dot{\mathbf{s}}_v = f(\mathbf{s}_v) \quad \mathbf{s}_v(0) = \mathbf{s}_0 \quad (10)$$

As discussed in Section 3, the trim states adopted by Level 2 simulations are generally periodic in nature so that:-

$$f(\mathbf{s}_v(t+T)_{trim}) = f(\mathbf{s}_v(t)_{trim})$$

represents the total periodicity of the solution to Equation 10. Alternatively, the definition introduced in Section 3 can be exploited to express the partial periodicity of the trim state:-

$$f(\mathbf{s}_v(t+T/n)_{trim}) = P_v f(\mathbf{s}_v(t)_{trim}).$$

In addition, the system matrix evaluated by linearisation, A , reflects this property and is also periodic in the trim:-

$$A(t+T) = A(t)$$

In fact, the partial periodicity condition may be introduced to show that:-

$$A(t+T/n)_{trim} = P_v A(t)_{trim} P_v^{-1}. \quad (11)$$

The generally accepted approach [5] for stability analysis of Level 2 simulations is to obtain an approximate linearisation of the periodic system by evaluating an *averaged* system matrix, \bar{A} , through one full period of the model states:-

$$\bar{A} = \frac{1}{nstps} \sum_{i=0}^{nstps-1} A(t_i)$$

Eigen-analysis of this *averaged* system matrix, \bar{A} , then yields an estimate to the stability of the full non-linear simulation model. Results presented in Section 6 will show that this approach has limitations when evaluating rotorcraft stability characteristics using Level 2 simulations and is particularly unreliable when identifying the higher order modes of the system. A more rigorous approach is found in classic Floquet theory which is specifically derived to assess the stability characteristics of periodic systems such as that given by Equation 10. A detailed discussion on classic Floquet theory is provided by Pontryagin [9]. Floquet theory was first applied to rotorcraft simulation models by Peters and Hohenemser [10] and is described by McVicar and Bradley [11]. The following section will present a novel technique that exploits the partial periodicity condition given by Equation 11 to produce an efficient enhancement of classic Floquet theory which is specific to Level 2 simulations. A similar, independently developed, enhancement of classical Floquet theory is reported by Peters [13].

5.1 Partial Floquet Stability Analysis of Level 2 Simulations

Partial Floquet theory considers the following (controls fixed) linear system:-

$$\dot{\mathbf{s}}_v = A(t)\mathbf{s}_v$$

where the system matrix obeys the partial periodic relationship given by Equation 11:-

$$A(t + T/n) = P_v A(t) P_v^{-1}.$$

Now, let the solution of:-

$$\dot{\mathbf{s}}_v = A(t)\mathbf{s}_v; \quad 0 < t < T/n; \quad \mathbf{s}_v(0) = \mathbf{e};$$

give:-

$$\mathbf{s}_v(T/n) = \mathbf{f}.$$

Since there is a matrix S , (which we will term the Partial Floquet Transition Matrix) found from m linearly independent solutions such that:-

$$S\mathbf{e} = \mathbf{f}$$

for all \mathbf{f} we can write:-

$$\mathbf{s}(T/n) = S\mathbf{e}.$$

Then the problem for the next segment may be expressed as:-

$$\dot{\mathbf{s}}_v = A(t)\mathbf{s}_v; \quad T/n < t < 2T/n; \quad \mathbf{s}_v(T/n) = \mathbf{f} = S\mathbf{e};$$

to be solved for $\mathbf{s}(2T/n)$. Application of the partial periodicity condition, given by Equation 11, leads to the form:-

$$\dot{\mathbf{s}}_v = P_v A(t - T/n) P_v^{-1} \mathbf{s}_v; \quad T/n < t < 2T/n; \quad \mathbf{s}_v(T/n) = \mathbf{f} = S\mathbf{e};$$

to be solved for $\mathbf{s}(2T/n)$. This may also be written:-

$$P_v^{-1} \dot{\mathbf{s}}_v = A(t - T/n) P_v^{-1} \mathbf{s}_v; \quad T/n < t < 2T/n; \quad P_v^{-1} \mathbf{s}_v(T/n) = P_v^{-1} S\mathbf{e}; \quad (12)$$

to find $P_v^{-1} \mathbf{s}_v(2T/n)$. The solution to Equation 12 is equivalent to solving:-

$$\dot{\mathbf{s}}_v = A(t)\mathbf{s}_v; \quad 0 < t < T/n; \quad \mathbf{s}_v(0) = P_v^{-1} \mathbf{f} = P_v^{-1} S\mathbf{e} \quad (13)$$

to find $\mathbf{s}(T/n)$. From the linearity of the problem, the solution to Equation 13 is:-

$$\mathbf{s}_v(T/n) = S P_v^{-1} \mathbf{f} = S P_v^{-1} S\mathbf{e}$$

and so Equation 12 has the solution:-

$$P_v^{-1} \mathbf{s}_v(2T/n) = S P_v^{-1} \mathbf{f} = S P_v^{-1} S\mathbf{e},$$

which is more conveniently written as:-

$$P_v^{-2} \mathbf{s}_v(2T/n) = (P_v^{-1} S)^2 \mathbf{e}.$$

Continued application of this argument leads to the result for a complete revolution:-

$$P_v^{-n} \mathbf{s}_v(T) = \mathbf{s}_v(T) = (P_v^{-1} S)^n \mathbf{e}, \quad (14)$$

having used the result that $P_v^{-n} = I_m$, the identity matrix of order m .

From Equation 14, it is apparent that the matrix given by $(P_v^{-1} S)^n$ performs the mapping of initial to final states across one period of the system. This matrix is therefore the Floquet Transition Matrix (which we will denote by R) of classic Floquet Theory:-

$$R = (P_v^{-1} S)^n. \quad (15)$$

Thus, Partial Floquet Theory has exploited the symmetry of the rotor to evaluate the R matrix by considering only a partial period of the system.

Eigen-analysis of the R matrix provides a description of the stability characteristics of the system. That is, the eigenvectors of R characterise the modal response of the system and the corresponding eigenvalues will reflect the growth of these modes across one period. Consequently, the eigenvalues of R must lie within the unit circle for stability.

For a more meaningful insight to the stability characteristics, the eigenvalues of the discretised system may be mapped to those of an equivalent continuous system. The damping of the k^{th} discrete eigenvalue, Λ_k , is mapped to the continuous plane by the following expression:-

$$\sigma_k = \frac{n}{T} \ln |\Lambda_k| \quad (16)$$

and its frequency is mapped by:-

$$\omega_k = \frac{n}{T} \tan^{-1} \left(\frac{\text{imag}(\Lambda_k)}{\text{real}(\Lambda_k)} \right) + n\Omega_r l \quad (17)$$

where the ambiguity in frequency, conveyed by the arbitrary integer l , is attributable to the periodicity of the \tan^{-1} function. As commented upon by Peters [13], it is apparent that the Partial Floquet technique offers an additional benefit over classical Floquet Theory when converting the eigenvalues from discrete to continuous planes. That is, the ambiguity introduced to the characteristic frequency component is improved from 1-per revolution, as occurs in classic Floquet, to n -per revolution in Partial Floquet.

5.2 Some Practical Considerations of Partial Floquet Analysis

The first stage in Partial Floquet Analysis is to trim the non-linear simulation model to the required flight state. It is essential that this trim is of high quality so that the system matrix obeys the partial periodic relationship given by Equation 11. The non-linear equations of motion are now integrated through $2\pi/n$ radians of rotor azimuth to establish the A matrices occurring in a partial period. If necessary, the full set of A matrices can be obtained by application of Equation 11. The Partial Floquet Transition Matrix, S , is then evaluated by integrating the linear model, given by Equation 10, through a partial period of the system using the identity matrix as the initial condition. Finally, the Floquet Transition Matrix, R , is obtained using Equation 15.

6 Trim and Stability Analysis of a Tilt-Rotor Simulation Model

In this section, the capabilities of the PPTA and Partial Floquet techniques are demonstrated by means of an investigation into the stability characteristics of the XV-15 tilt-rotor vehicle. In particular, this investigation will focus on the turning flight condition specified below:-

vehicle speed, V	100 Knots
vehicle sideslip angle, β	0°
vehicle turn rate, Ω	10°s^{-1}
vehicle angle of climb, γ	0°
nacelle incidence, γ_n	60° .

The first stage in the stability analysis is to trim the non-linear simulation model, TILTSTAB, to the specified flight condition and this process is now used to demonstrate the performance of the PPTA.

6.1 Performance of the Partial Periodic Trimmer

As stated in Section 5.1, the integrity of the Partial Floquet Stability analysis technique is dependent on the trimmed A matrix obeying the partial periodic relationship given by Equation 11. This condition will only be satisfied if the trim state obtained by the PPTA is of the highest quality. In order to ensure that Equation 11 is satisfied (and also to demonstrate the capabilities of the PPTA), an extremely stringent convergence criterion of $\pm 1\text{e-}12$ was imposed on all elements of the error vector, ϵ during the trimming phase; where ϵ is given by:-

$$\epsilon = \begin{bmatrix} \mathbf{s}_v(2\pi/n) - P_v \mathbf{s}_v(0) \\ \bar{\mathbf{x}} - \mathbf{x}_{\text{trim}} \end{bmatrix}.$$

In this example, the specified trim state was obtained in 10 iterations which represents very rapid convergence indeed given that the full set of initial conditions and control displacements have been ascertained to the 12th decimal place. From a practical viewpoint, however, the CPU time necessary to attain the trim is perhaps of greater interest than the associated number of iterations. When using the PPTA to trim a simulation with n blades per rotor, the rotor must be integrated through $2\pi/n$ radians to form each row of the Jacobian matrix. Consequently, for a model with 3 blades per rotor and 30 states (as in this case), each iteration will require 10 revolutions of rotor azimuth to complete: for the XV-15 in transition mode this corresponds to approximately 1.1 seconds of real-time simulation. It follows that, the PPTA would require 11 seconds of real-time simulation to produce the trim condition discussed in this section. (When implemented on a DEC Alpha 3000 model 400 platform, this requirement translated to 18.5 seconds CPU time). Hence, the PPTA is a very fast algorithm both in terms of its convergence characteristics and also the CPU time it requires to produce exceptionally high quality trim states.

Tables 1 and 2 provide a comparison between the start values input to the PPTA and the trimmed parameters obtained at the 10th iteration. With reference to these tables, it can be seen that an extremely poor set of start values were used in this example. In particular, errors of up to 267°s^{-1} exist between the start values for the initial flap rates and their corresponding trim values. Also, the start values used for the control states include very poor estimates for the longitudinal stick, lateral stick and pedal displacements (fully aft, fully left and fully left respectively). From this example, it is evident that the PPTA is capable of quickly producing very high quality trim states despite the use of exceptionally poor start values. It may therefore be concluded that the PPTA is robust to the quality of start values.

Figure 1 shows a comparison of the periodic trajectories produced for some examples of rigid body and rotor states at the start and end of a 120 second forward simulation. In each plot, the solid line depicts the trajectory produced during the first turn of the rotor (i.e. from $t=0$) and the crosses depict the corresponding trajectory produced during the final turn of the rotor (i.e. to $t=120$ seconds). With reference to this figure it is apparent that, despite the extended run time, the periodic trim state is maintained throughout the duration of the simulation. In fact, inspection of the time histories revealed that the periodic trajectories of all the model states are maintained to within the specified convergence criteria ($\pm 1\text{e-}12$) for the full 120 seconds of simulation. It is also interesting to note that the earth axis trajectory and groundtrack produced during the forward simulation describe an orbit which is perfectly circular in nature over a radius of 300 metres. Furthermore, as a 10 degree per second turn rate was specified as part of this trim condition, over 3 full orbits were completed during the forward simulation. Inspection of the vehicle trajectory revealed that, despite the large radius and extended simulation time, these orbits are coincident to within the 12th decimal place. Hence, it can be concluded that the trim state produced by the PPTA is of the highest quality with all of the model states maintaining their periodic trajectories throughout the duration of the extended simulation.

From the results presented in this section, it may be concluded that the PPTA is a very efficient and robust algorithm which is capable of producing high quality states to adverse areas of the flight envelope.

6.2 Stability Analysis of the XV-15 in Turning Flight

As discussed in Section 5, the widely adopted approach [5] for stability analysis of Level 2 simulations is to perform eigen-analysis of the averaged system matrix \bar{A} . The following results will show that, whilst this approach may adequately estimate the rigid body modes, it has limitations when considering the higher order modes of the system, which in this case are the rotor modes.

6.2.1 Comparison Between Eigenvalues of the Floquet Transition Matrix and Average A Matrix in the Discrete Plane

Figure 2 and Table 3 provide a comparison between the eigenvalues of the Floquet Transition Matrix and average A matrix in the discrete plane. Before performing this comparison, the k^{th} eigenvalue of the continuous (average A) system was mapped to that of an equivalent discrete system by the standard expression:-

$$\Lambda_k = e^{(\sigma_k T)} \cos(T\omega_k) + j e^{(\sigma_k T)} \sin(T\omega_k)$$

where, σ_k is the real part of the continuous eigenvalue and ω_k is its imaginary part.

When discussing the results presented in Figure 2, it is most convenient to classify the modes according to the following three categories:-

1. rigid body modes

2. induced flow modes
3. flap modes

and each of these is now discussed in turn starting with the rigid body modes.

1. **Rigid Body Modes:-** With reference to Figure 2 and Table 3 it is evident that very good agreement exists between the average A and Floquet techniques for the classic 6 DOF rigid body modes. In fact, with one exception, the Floquet eigenvalues for the rigid body modes lie within 1% of their counterparts established by average A analysis.

2. **Induced Flow Modes:-** Figure 2 shows that the average A and Floquet techniques establish similar distributions for the 6 induced flow modes (3 for the right rotor and 3 for the left rotor). After inspection of the corresponding eigenvectors, these modes may be classified as follows:-

- lateral harmonic induced flow mode for the right rotor
- lateral harmonic induced flow mode for the left rotor
- uniform/longitudinal harmonic induced flow mode for the right rotor
- uniform/longitudinal harmonic induced flow mode for the left rotor.

The structure of the Peters-HaQuang dynamic inflow model [7] is responsible for the distribution of induced flow modes described above. In particular, the dynamic gain matrix couples the response of the uniform and longitudinal induced flow states with the rotor thrust and aerodynamic pitching moments. Hence, the modal response of the uniform and longitudinal induced flow states is coupled producing the two pairs (one pair for the right rotor, one pair for the left rotor) of complex modes described above. Conversely, the lateral induced flow is driven purely by the aerodynamic rolling moment and hence its response takes the form of a single real mode for each rotor.

From Table 3 one can see that disparities of up to 32% exist between the Floquet and average A eigenvalues for the induced flow modes. Hence, each technique is establishing the same distribution of eigenvalues for these modes but the level of correlation is degraded over that obtained for the rigid body modes.

3. **Flap Modes:-** With reference to Figure 2 and Table 3 it is apparent that the average A and Partial Floquet techniques establish differing characteristics for the flap modes. More specifically, the flap modes produced by Partial Floquet Analysis may be considered to occur in 3 distinct groups:-

- | | | |
|----------------|--------------------------|---|
| <i>Group 1</i> | 2 pairs of complex modes | (at $-0.2868 \pm 0.6061j$ and $-0.2816 \pm 0.6099j$) |
| <i>Group 2</i> | 2 pairs of complex modes | (at $-0.3648 \pm 0.5262j$ and $-0.3608 \pm 0.5281j$) |
| <i>Group 3</i> | 4 real flap modes | (between -0.6423 and 0.7429) |

whereas the average A flap modes occur in 2 distinct groups:-

- | | | |
|----------------|--------------------------|--|
| <i>Group 1</i> | 2 pairs of complex modes | (at $-0.2918 \pm 0.5986j$ and $-0.2867 \pm 0.6027j$) |
| <i>Group 2</i> | 4 pairs of complex modes | (at $-0.2932 \pm 0.5368j$ and $-0.2964 \pm 0.5339j$). |

Correlation between the average A and Partial Floquet techniques is very good for the *Group 1* flap modes with the real parts lying within 2% and the imaginary parts within 1.5%. Figure 4 provides phasor representations of eigenvectors produced by average A and Partial Floquet Analysis for one of the *Group 1* flap modes. With reference to this figure, it can be seen that both techniques are establishing a similar shape for this mode. In particular, the modal response is dominated by the flap states of the right rotor with some excitation also present for the right rotor's induced flow states. The response for each of the dominant flap states are in phase and the main induced flow contribution is provided by the uniform component, therefore, it may be concluded that this is a coning mode for the right rotor. Similar analysis for the remaining *Group 1* flap mode reveals that it represents a coning mode for the left rotor. Hence, the *Group 1* modes, as identified by both Partial Floquet and Average A analysis, represent 1 pair of complex coning modes for the right rotor and 1 pair of complex coning modes for the left rotor.

It is evident that Partial Floquet and Average A analysis establish differing distributions for the *Group 2* flap modes. Table 3 and Figure 2 reveal that the average A group comprises 4 pairs of complex flap modes (distributed as 2 repeated pairs) whereas the Partial Floquet group comprises only 2 pairs of complex modes. Figure 5 provides phasor representations of eigenvectors produced by average A and Partial Floquet Analysis for one of the *Group 2* flap modes. Both eigenvectors shown in this figure are dominated by the flap states

of the right rotor with a 120° phase shift being established between the response of the blades in each case. The presence of this phase shift suggests that the *Group 2* modes are either disc progressing or disc subsidence modes. In fact, a multi-blade transformation was used to analyse the response of the rotor disc plane to the *Group 2* modes and revealed that these may be classified as disc progressing modes.

With reference to the phasor diagrams shown in Figure 5, it can be seen that average *A* analysis identifies that the response of the disc progressing modes involves purely the flap states for the one rotor. Conversely, Floquet analysis establishes fairly strong excitation of the induced flow states and some excitation of the other rotor's flap states as part of the modal response. Hence, it should be noted that Floquet and average *A* analysis are identifying differing mode shapes for the disc progressing modes.

Partial Floquet Analysis alone establishes the 4 real flap modes which form the *Group 3* set. Analysis of the modal response of the rotor disc plane, again using a multi-blade transformation, allows us to classify these modes as disc subsidence modes.

With reference to Figure 2, it can be seen that the full set of eigenvalues lie within the unit circle and therefore all modes of the vehicle are stable in this regime. It is perhaps apparent that the discrete plane gives only a fairly qualitative insight to the stability characteristics of the vehicle. For example, one can deduce that the rigid 6 DOF modes which lie at the periphery of the unit circle are lightly damped whereas the inflow modes lying near the origin are heavily damped. However, a more detailed quantitative appraisal of the modal damping is extremely difficult from this plot. Furthermore, the discrete plane yields only very limited qualitative information on the modal frequency content, in fact, one can only readily determine whether the modes are complex or real. For a comparison in more familiar terms one must map the discretised eigenvalues, using Equations 16 and 17, to those of an equivalent continuous system.

6.2.2 Comparison Between Eigenvalues of the Floquet Transition Matrix and Average *A* Matrix in the Continuous Plane

Figure 3 and Table 4 provide a comparison between the eigenvalues of the Floquet Transition Matrix and Average *A* matrix in the continuous plane. When generating this plot, only the fundamental frequency of the Floquet eigenvalues were considered as it was felt that a shift of $3\Omega_r$, in this case 180 rads^{-1} , in the angular velocity would produce unrepresentative eigenvalues of the system. From the results presented here, it is clear that the continuous plane provides a more meaningful insight to the characteristics of all the vehicle's modes. In particular, one can readily determine the modal frequency and time to half amplitude from inspection of the continuous eigenvalues and this is of great assistance when establishing the nature of the modes.

From Figure 3 and Table 4 it is clear that both average *A* and Floquet analysis are establishing similar characteristics for the 6 DOF rigid body modes where, in most cases, the respective eigenvalues lie within 10%.

The disparities occurring between average *A* and Floquet rotor modes are clearly visible in the continuous plane. With reference to Figure 3 one can again see that differing distributions are identified by average *A* and Floquet analysis for the flap modes. Also, it is apparent that the Floquet induced flow modes are, in all cases, more heavily damped than their counterparts established by average *A* analysis.

7 Analysis of Floquet and Average *A* Flap Modes

As stated in the introduction to this paper, high bandwidth control systems are now being developed for the stability and control augmentation of the next generation of rotorcraft. It is also noted that a detailed knowledge of the vehicle higher order dynamics is essential in order to ensure the integrity of these new high bandwidth control systems. Clearly, any high bandwidth control system designed around an incorrect evaluation of the rotor modes would be of questionable integrity and this could have serious implications on the handling qualities of the augmented vehicle. Hence, it is important to determine which of the above analysis techniques is establishing the correct distribution of flap modes.

The two partitions (1 for the right rotor, 1 for the left rotor) of $A(t)$ that contain the flap derivatives have

the following structure:-

$$A(t)_{flap} = \begin{bmatrix} \frac{\partial \dot{\beta}_1}{\partial \beta_1} & \frac{\partial \dot{\beta}_1}{\partial \beta_1} & \dots & \dots & \frac{\partial \dot{\beta}_1}{\partial \beta_3} \\ \frac{\partial \dot{\beta}_1}{\partial \beta_1} & \frac{\partial \dot{\beta}_1}{\partial \beta_1} & \dots & \dots & \frac{\partial \dot{\beta}_1}{\partial \beta_3} \\ \vdots & \vdots & \dots & \dots & \vdots \\ \frac{\partial \dot{\beta}_3}{\partial \beta_1} & \frac{\partial \dot{\beta}_3}{\partial \beta_1} & \dots & \dots & \frac{\partial \dot{\beta}_3}{\partial \beta_3} \end{bmatrix}$$

where:-

$$\left. \begin{array}{l} \frac{\partial \dot{\beta}_n}{\partial \beta_m} = 0 \quad \frac{\partial \dot{\beta}_n}{\partial \beta_n} = 0 \\ \frac{\partial \dot{\beta}_n}{\partial \beta_m} = 0 \quad \frac{\partial \dot{\beta}_n}{\partial \beta_n} = 0 \end{array} \right\} n \neq m$$

$$\begin{array}{l} \frac{\partial \dot{\beta}_n}{\partial \beta_n} = 0 \quad (\text{constant}) \\ \frac{\partial \dot{\beta}_n}{\partial \beta_n} = 1 \quad (\text{constant}) \end{array}$$

and, in this case:-

$$\frac{\partial \ddot{\beta}_n}{\partial \beta_n} = \begin{cases} -3614s^{-2} & \text{right rotor} \\ -3639s^{-2} & \text{left rotor} \end{cases} \quad (\text{mean values, periodic})$$

$$\frac{\partial \ddot{\beta}_n}{\partial \beta_n} = \begin{cases} -28s^{-1} & \text{right rotor} \\ -28s^{-1} & \text{left rotor} \end{cases} \quad (\text{mean values, periodic})$$

Figure 6 depicts the full periodicity of the dominant flap derivatives, $\frac{\partial \dot{\beta}_n}{\partial \beta_n}$, for the right rotor. When generating these plots, the system matrix, $A(t)$, was evaluated for a partial revolution of rotor azimuth and the partial periodicity condition, given by Equation 11, used to provide the full periodic trajectories. As one would perhaps expect, these derivatives all exhibit the same periodicity (peak-to-peak 800 s^{-2} , mean -3614 s^{-2}) with a phase shift of $2\pi/n$ of rotor azimuth occurring between the path associated with each consecutive blade.

Floquet stability analysis captures the effects of the periodicity and phase shift shown in Figure 6 when the periodic A linear model is integrated through a partial revolution of rotor azimuth. The Floquet transition matrix, R , therefore, provides an exact evaluation of the growth in the model states across one period of the linear system. Hence, eigen-analysis of the R matrix will yield an accurate set of flap modes for the periodic system.

Conversely, the average A approach does not encompass the periodicity of the state derivatives but instead adopts their mean values. This approximation has implications for all the identified modes but has greatest impact on the flap modes as the flapping derivatives have the largest peak-to-peak amplitude (e.g. 800 s^{-2} for $\frac{\partial \dot{\beta}_n}{\partial \beta_n}$ as opposed to $5\text{ms}^{-2}\text{rad}^{-1}$ for $\frac{\partial \dot{w}_n}{\partial \beta_n}$). The A_{flap} partitions for each rotor are now dominated by the mean $\frac{\partial \dot{\beta}_n}{\partial \beta_n}$ derivatives and these values will be repeated for each blade. For example, the A_{flap} partition for the right rotor is given by:-

$$A_{flap} = \begin{bmatrix} 0 & 1 & 0 & 0 & 0 & 0 \\ -3614 & -28 & 0 & 0 & 0 & 0 \\ 0 & 0 & 0 & 1 & 0 & 0 \\ 0 & 0 & -3614 & -28 & 0 & 0 \\ 0 & 0 & 0 & 0 & 0 & 1 \\ 0 & 0 & 0 & 0 & -3614 & -28 \end{bmatrix}$$

It is this block diagonal structure of the A_{flap} partition which leads to the generation of repeated eigenvalues in the average A flap modes. In fact, eigen-analysis of the partition quoted above yields 3 pairs of repeated complex modes whose eigen-value is equal to that of the right rotor progressing modes given in Table 4.

Furthermore, the average A system matrix, \bar{A} , has sacrificed the periodicity and relative phasing of the dominant flap derivatives, $\frac{\partial \dot{\beta}_n}{\partial \beta_n}$, shown in Figure 6. The average A linear model is, therefore, a time invariant system in which the flapping derivatives experienced by the blades are constant (the respective mean values) and independent of the blades' individual azimuthal positions. This approximation is of greatest significance

in the context of the progressing and regressing modes where the modal response is periodic with a phase shift between the motion of each blade. In order to produce this behaviour accurately, the linear model must include the correct phasing and periodicity of the flap derivatives. Clearly, this information is lost during the averaging process and therefore the time-invariant model cannot correctly generate the progressing and regressing modes.

To verify the preceding discussions, eigenvectors for each of the Floquet and average A flap modes were superimposed onto the trimmed state vector and input to the full non-linear simulation model. The resulting time histories were then analysed to ascertain which set of responses were exhibiting transient behaviour consistent with the corresponding eigenvalues. The observations presented in the following section summarise the results obtained.

7.1 Response of Non-Linear Simulation Model to A Floquet Disc Subsidence Mode

The four *Group 3* or real disc subsidence modes identified by Floquet Analysis are of key interest in this exercise as their presence indicates that eigen-analysis of the average A matrix has not fully captured the higher order modes of the system. In the following example, the eigenvector for one of the symmetric disc subsidence modes ($\lambda=-8.6354$, $t_{0.5}=0.0803$ seconds) was superimposed onto the trimmed state vector and input to the full non-linear simulation model. For comparison, this eigenvector was also input to the linearised model used when evaluating the Floquet Transition Matrix, that is, the model which incorporates the Partial Periodic condition as given by Equation 11. The results obtained are exemplified by the time histories for the right rotor states provided in Figure 7.

With reference to this figure, it can be seen that the linear model has accurately replicated the behaviour of the full non-linear simulation with both sets of time histories being virtually coincident for all states. Most significantly, the transient response of the non-linear model is consistent with both the identified modal damping (characterised by the Floquet eigenvalue) and with the mode shape (characterised by the Floquet eigenvector shown in Figure 4). In addition, there is negligible cross excitation of any other modes. It can be concluded that the real disc subsidence modes are indeed true modes of the system and thus, Floquet analysis has established accurately the higher order rotor modes.

7.2 Response of Non-Linear Simulation Model to An Average A Disc Progressing Mode

In this case, the modes of greatest interest are the two pairs of repeated progressing modes (occurring at $\lambda=-13.8873 \pm 57.1891j$ and $\lambda=-13.9316 \pm 58.4953j$) as coincident modes of this type were not identified by Floquet analysis. The eigenvector corresponding to one of the progressing modes for the right rotor was superimposed onto the trimmed state vector and input to the full non-linear simulation model. For comparison, this mode was also input to the linearised model which adopts the average A matrix as the system matrix. The time histories for the right rotor states are provided in Figure 8 and typify the results obtained.

From this figure, it is evident that the level of correlation between non-linear and linear simulation models is poor when compared to the previous Floquet example. With reference to the time histories produced by the linear model it can be seen that this response is commensurate with the identified mode. Clearly, there is no excitation of the inflow states which maintain their periodic trim state throughout the simulation and this is in accordance with the identified mode shape - as shown in Figure 5 and discussed in Section 6.2.1. Also, the transient responses of the blade flap states are consistent with the period and time to half amplitude indicated by the modal eigenvalue. Therefore, as one would perhaps expect, the higher order modes of the linear simulation model have been identified accurately by eigen-analysis of the average A matrix. Of much greater significance, however, is the fact that the response of the non-linear simulation does not conform with the characteristics of the identified mode. Although the blade responses do appear to follow the transient prescribed by the modal eigenvalue, there is strong coupling to the induced flow states and this is inconsistent with the identified mode shape. In particular, one can see transient oscillations in excess of 1 ms^{-1} on the harmonic induced flow states. In fact, it would appear that one of the real disc subsidence modes (as identified by Floquet analysis) has been excited in the transient response of the induced flow states. Hence, it may be concluded that the average A linear model does not accurately replicate the response of the full non-linear simulation and that eigen-analysis of the average A matrix has failed to identify the higher order rotor modes of the full non-linear simulation.

8 Conclusions

A specialised, Partial Periodic, trimming algorithm (PPTA) was developed for application to the latest generation of rotorcraft simulation models. This algorithm is capable of simultaneously obtaining the initial conditions and control displacements necessary to produce a specified periodic flight state and achieves computational economy by exploiting the symmetry of the rotor. Furthermore, the PPTA is particularly robust to the quality of start values and, consequently, there is no recourse to damping parameters which would slow the convergence of the scheme. The full non-linear simulation model is used by the PPTA and hence exactly the same model structure is used during the trim and forward simulation phases. This feature results in trim states of the highest quality which are precisely maintained throughout forward simulations of extended duration.

The partial periodicity relationships were then used to produce an efficient development of classical Floquet techniques for analysing rotorcraft stability characteristics using advanced simulation models. The resulting method, termed Partial Floquet Analysis, was used to assess tilt-rotor stability characteristics from an individual blade simulation model. During the course of this work, the modes identified by Partial Floquet analysis were compared with those produced by eigen-analysis of the averaged system matrix. It was found that reasonably good correlation existed between the two approaches for the 6 DOF rigid body modes, however, differing characteristics were established for the higher order rotor modes. Injection of the flap mode eigenvectors to the full non-linear simulation model exposed limitations in the average A approach when analysing the higher order modes of the system. However, this exercise verified that Floquet analysis had identified accurately the higher order modes of the full non-linear simulation model.

9 Acknowledgements

The trimming algorithm reported in this paper was originally developed by the authors at the University of Glasgow under a SERC CASE award in collaboration with the Defence Research Agency (Bedford).

References

- [1] Aponso, B. L., Johnston, D. E., Johnston, W. A., Magdaleno, R. E., "Identification of Higher Order Helicopter Dynamics Using Linear Modelling Methods", *Journal of the American Helicopter Society*, July 1994, pp. 3 - 11
- [2] Padfield, G. D., "Theoretical Modelling of Helicopter Flight Mechanics: Development and Validation", *Proceedings of the 16th ICAS Conference*, London, 1988
- [3] Anon, "Aeronautical Design Standard, Handling Qualities Requirements for Military Rotorcraft", ADS-33C, August 1989
- [4] McVicar, J. S. G., Bradley, R., "A Generic Tilt-Rotor Simulation Model with Parallel Implementation and Partial Periodic Trim Algorithm", *Proceedings of the Eighteenth European Rotorcraft Forum*, Avignon, France, September 1992
- [5] Hansen, R. S., "Toward a Better Understanding of Helicopter Stability Derivatives", *Journal of the American Helicopter Society*, January 1984, pp.15 - 24
- [6] Glauert, H., "A General Theory of the Autogyro", ARC RI&M 1111, 1926
- [7] Peters, D. A., HaQuang, N., "Dynamic Inflow for Practical Applications", *Journal of the American Helicopter Society*, Technical Note, 1988
- [8] McVicar, J. S. G., Bradley, R., "Robust and Efficient Trimming Algorithm for Application to Advanced Mathematical Models of Rotorcraft", *Journal of Aircraft*, Volume 32, Number 2, pp 439-442
- [9] Pontryagin, L. S., "Ordinary Differential Equations", Addison-Wesley Publishing Company, Reading, Massachusetts, 1962
- [10] Peters, D. A., Hohenemser, K. H., "Application of the Floquet Transition Matrix to Problems of Lifting Rotor Stability", *Journal of the American Helicopter Society*, April 1971, pp. 25 - 33

- [11] McVicar, J. S. G., Bradley, R., "Efficient Algorithms for Trimming and Stability Analysis of Advanced Rotorcraft Simulations", *Proceedings of the CEAS Symposium on Simulation Technology*, Delft, The Netherlands, October 1995
- [13] Peters, D. A., "Fast Floquet Theory and Trim for Multi-Bladed Rotorcraft", *Proceedings of the 51st Annual Forum of the American Helicopter Society*, Fort Worth, Texas, May 1995, pp. 444 - 459

state	right rotor		left rotor	
	start value (1st Iteration)	trim value (10th Iteration)	start value (1st Iteration)	trim value (10th Iteration)
β_1 (deg)	0	-3.5385	0	-3.3985
$\dot{\beta}_1$ (degs ⁻¹)	0	-14.6212	0	-58.2782
β_2 (deg)	0	3.6736	0	2.9564
$\dot{\beta}_2$ (degs ⁻¹)	0	256.3200	0	267.1903
β_3 (deg)	0	4.2007	0	4.6576
$\dot{\beta}_3$ (degs ⁻¹)	0	-242.9455	0	-210.5260
v_0 (ms ⁻¹)	20.0	3.1796	20.0	2.8685
v_{1s} (ms ⁻¹)	0	0.6176	0	-0.4892
v_{1c} (ms ⁻¹)	0	3.1162	0	3.2408

Table 1: Comparison Between Start Values and Trimmed Initial Conditions for Rotor States

state	start value (1st Iteration)	trim value (10th Iteration)
u_a (ms ⁻¹)	60	48.2315
v_a (ms ⁻¹)	0	0.0000
w_a (ms ⁻¹)	0	16.9142
p (degs ⁻¹)	0	-2.4467
q (degs ⁻¹)	0	6.7198
r (degs ⁻¹)	0	6.9689
θ (deg)	0	14.1469
ϕ (deg)	0	44.0452
θ_{occ} (deg)	45.3837	49.7707
X_{long} (% fwd)	0	40.0753
X_{lat} (% right)	0	50.9732
X_{pedal} (% right)	0	60.0465

Table 2: Comparison Between Start Values and Trimmed Initial Conditions for the Body States and the Control States

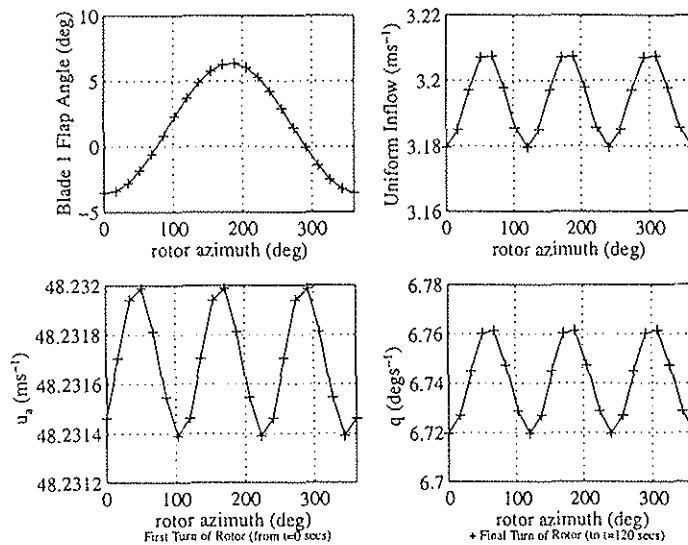


Figure 1: Comparison Between Periodic Trajectories Produced at Start and End of 120 Second Simulation

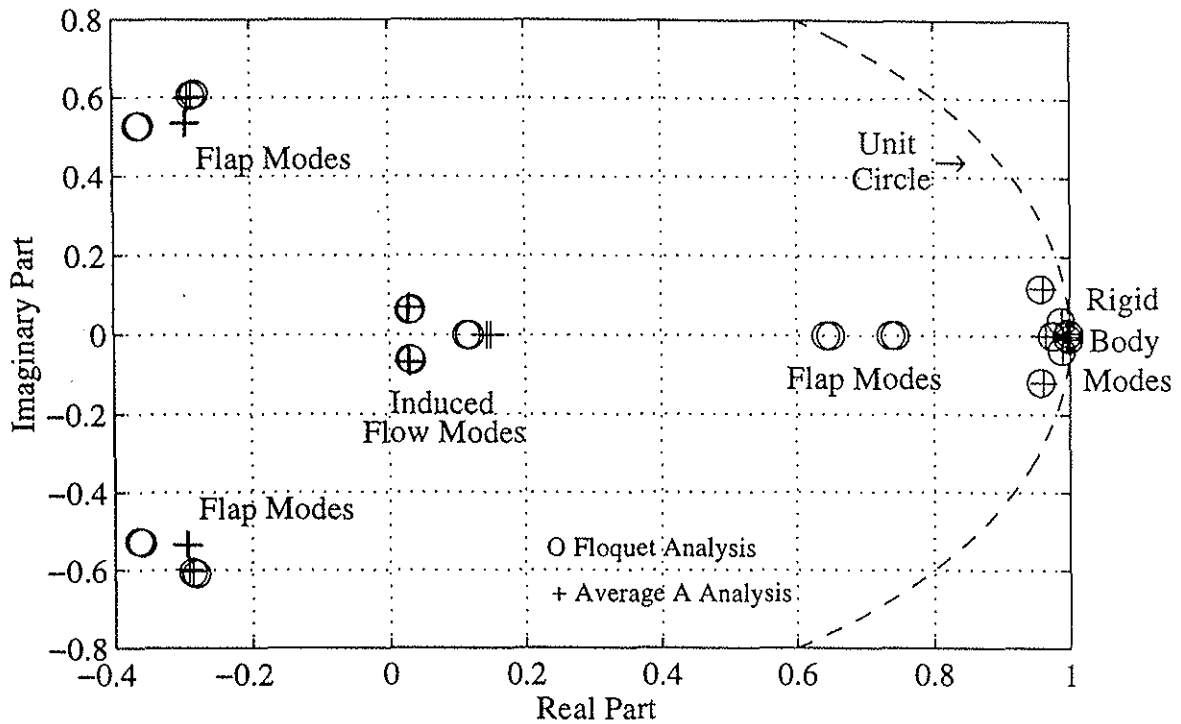


Figure 2: Comparison Between Eigenvalues of the Floquet Transition Matrix and Average A Matrix in the Discrete Plane

mode	Floquet Eigenvalue	Average A Eigenvalue
spiral	0.9735	0.9644
roll divergence	0.9944	0.9948
phugoid	$0.9979 \pm 0.0077j$	$0.9973 \pm 0.0076j$
Dutch roll	$0.9877 \pm 0.0371j$	$0.9888 \pm 0.0351j$
short period	$0.9571 \pm 0.1191j$	$0.9609 \pm 0.1194j$
lateral inflow - left rotor	0.1125	0.1485
lateral inflow - right rotor	0.1171	0.1424
longitudinal/uniform inflow - left rotor	$0.0294 \pm 0.0617j$	$0.0265 \pm 0.0673j$
longitudinal/uniform inflow - right rotor	$0.0327 \pm 0.0644j$	$0.0296 \pm 0.0705j$
anti symmetric disc subsidence	0.7429	-
symmetric disc subsidence	0.7366	-
anti symmetric disc subsidence	0.6423	-
symmetric disc subsidence	0.6496	-
coning - left rotor	$-0.2868 \pm 0.6061j$	$-0.2918 \pm 0.5986j$
coning - right rotor	$-0.2816 \pm 0.6099j$	$-0.2867 \pm 0.6027j$
progressing - right rotor	$-0.3648 \pm 0.5262j$	$-0.2932 \pm 0.5368j$
progressing - left rotor	$-0.3608 \pm 0.5281j$	$-0.2964 \pm 0.5339j$
progressing - right rotor	-	$-0.2932 \pm 0.5368j$
progressing - left rotor	-	$-0.2964 \pm 0.5339j$

Table 3: Floquet and Average A Eigenvalues in the Discrete Plane

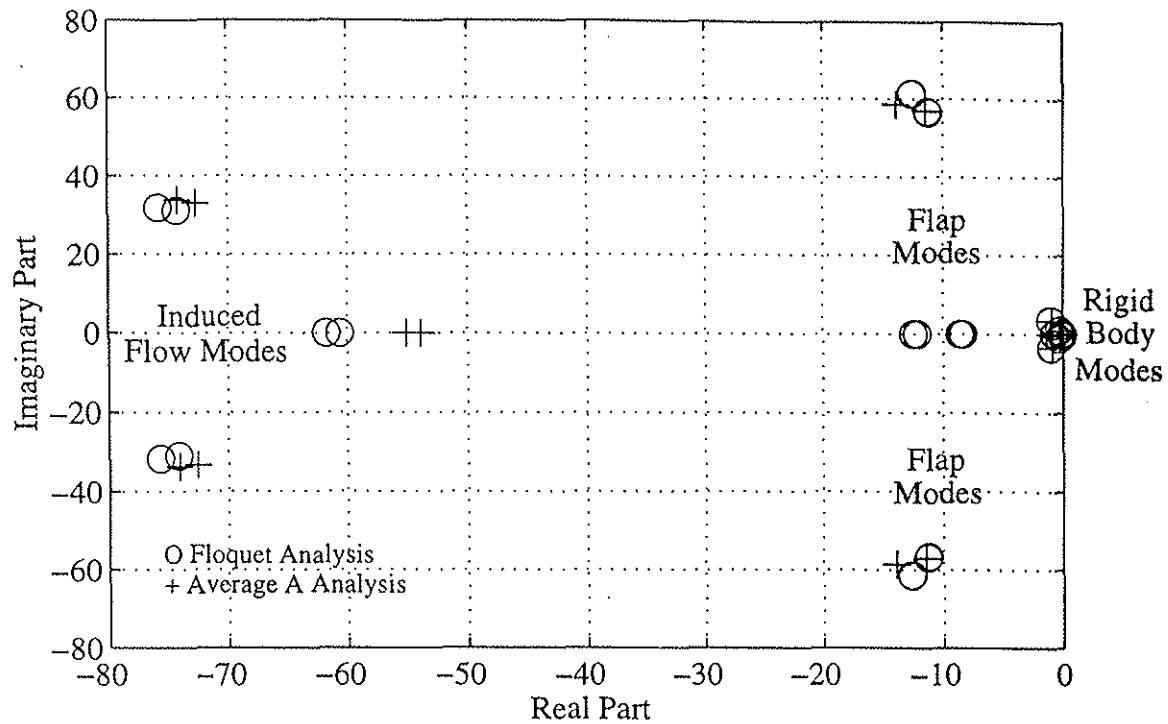


Figure 3: Comparison Between Eigenvalues of the Floquet Transition Matrix and Average A Matrix in the Continuous Plane

mode	Floquet Eigenvalue	Average A Eigenvalue
spiral	-0.7598	-1.0238
roll divergence	-0.1601	-0.1481
phugoid	$-0.0594 \pm 0.2178j$	$-0.0754 \pm 0.2153j$
Dutch roll	$-0.3288 \pm 1.0601j$	$-0.2997 \pm 1.0021j$
short period	$-1.0215 \pm 3.4978j$	$-0.9094 \pm 3.4918j$
lateral inflow - left rotor	-61.7272	-53.8820
lateral inflow - right rotor	-60.5921	-55.0538
longitudinal/uniform inflow - left rotor	$-75.7937 \pm 31.7934j$	$-74.1802 \pm 33.7700j$
longitudinal/uniform inflow - right rotor	$-74.2510 \pm 31.0880j$	$-72.6521 \pm 33.1521j$
anti symmetric disc subsidence	-8.3950	-
symmetric disc subsidence	-8.6354	-
anti symmetric disc subsidence	-12.5084	-
symmetric disc subsidence	-12.1860	-
coning - left rotor	$-11.2931 \pm 56.8593j$	$-11.4871 \pm 57.1891j$
coning - right rotor	$-11.2373 \pm 56.5953j$	$-11.4234 \pm 56.9201j$
progressing - right rotor	$-12.5952 \pm 61.5003j$	$-13.8875 \pm 58.4953j$
progressing - left rotor	$-12.6263 \pm 61.3048j$	$-13.9316 \pm 58.6909j$
progressing - right rotor	-	$-13.8875 \pm 58.4953j$
progressing - left rotor	-	$-13.9316 \pm 58.6909j$

Table 4: Floquet and Average A Eigenvalues in the Continuous Plane

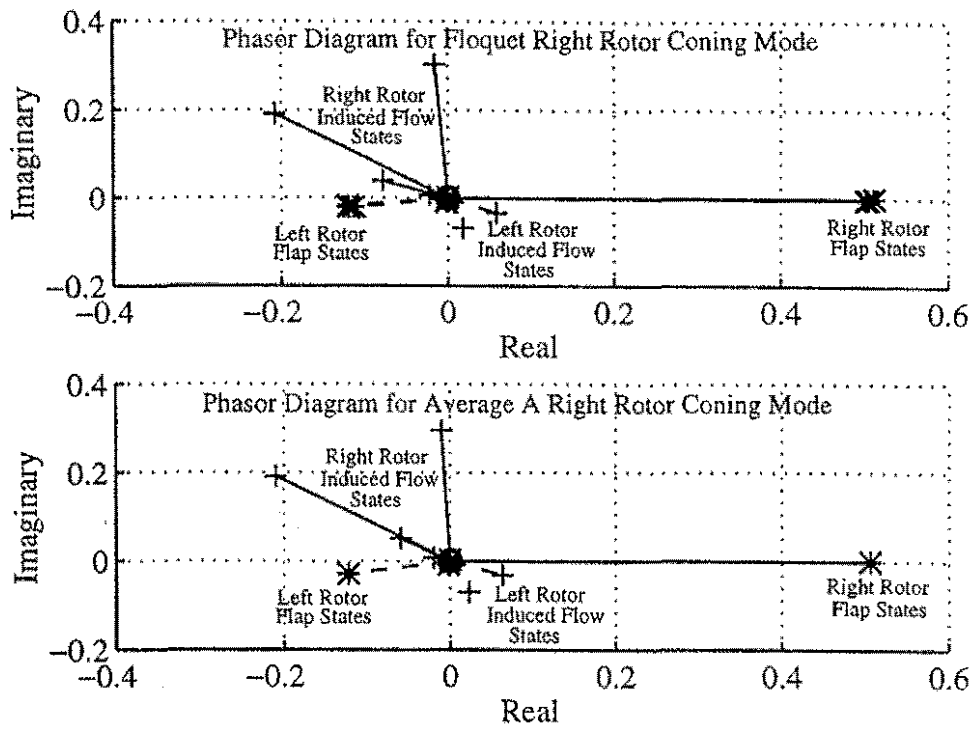


Figure 4: Phasor Diagrams of the Partial Floquet and Average A Right Rotor Coning Modes (at $\lambda = -11.2373 \pm 56.5953j$ and $\lambda = -11.4234 \pm 56.9201j$ respectively)

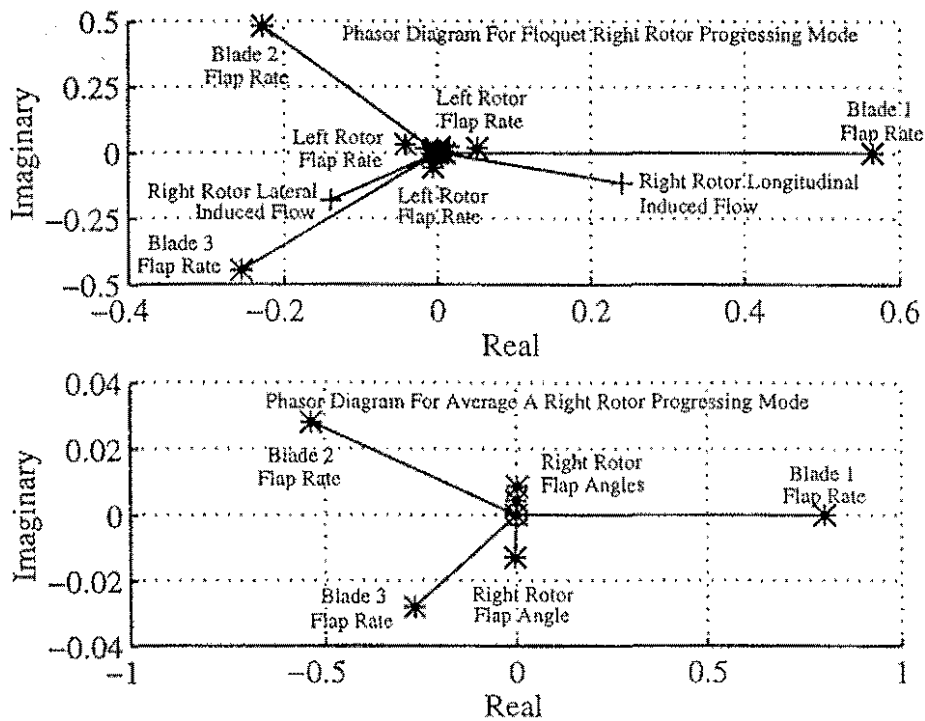


Figure 5: Phasor Diagrams of the Partial Floquet and Average A Right Rotor Progressing Modes (at $\lambda = -12.5952 \pm 61.5003j$ and $\lambda = -13.8875 \pm 58.4953j$ respectively)

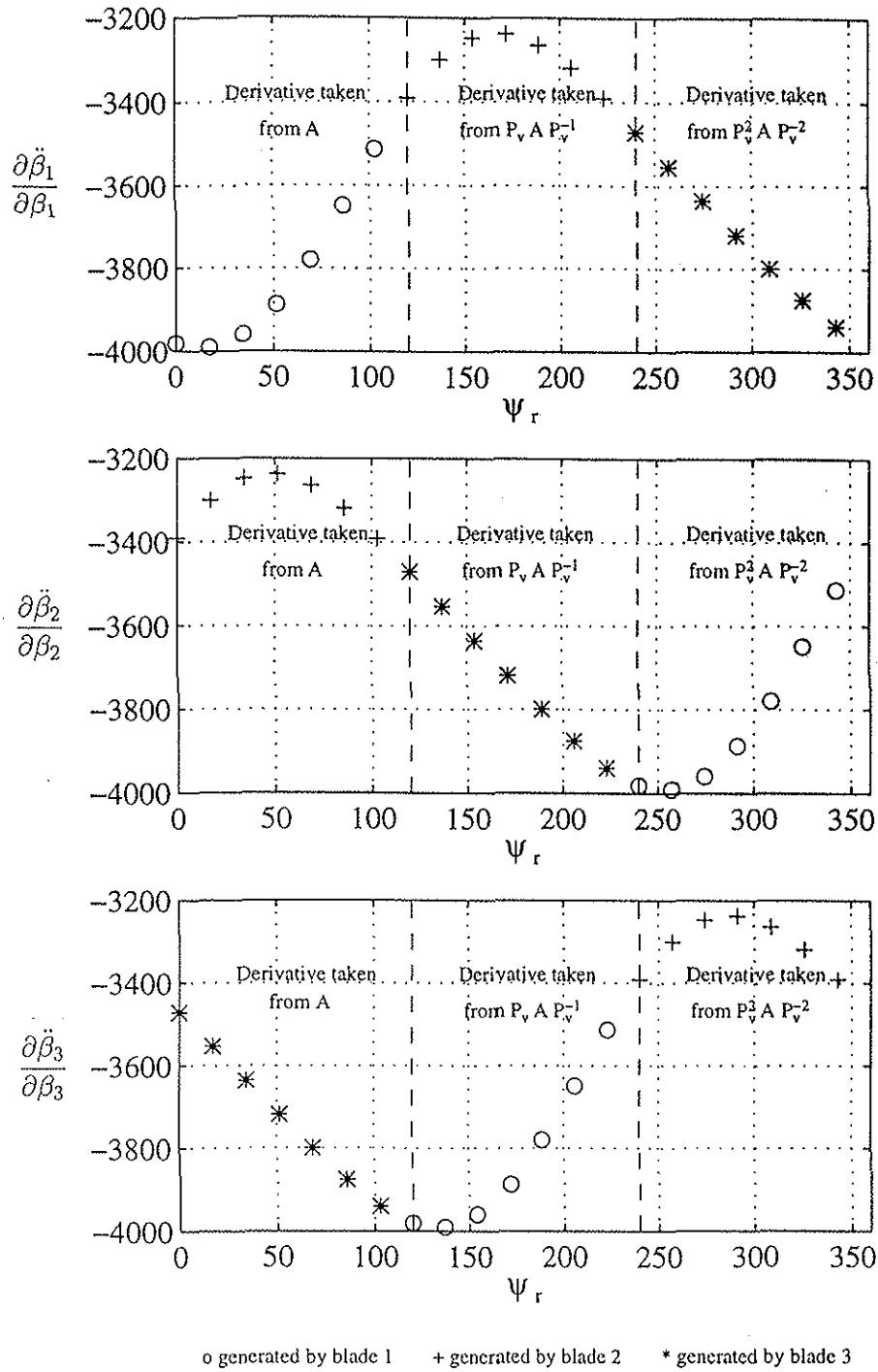


Figure 6: Flapping derivatives against rotor azimuth for one turn of the rotor

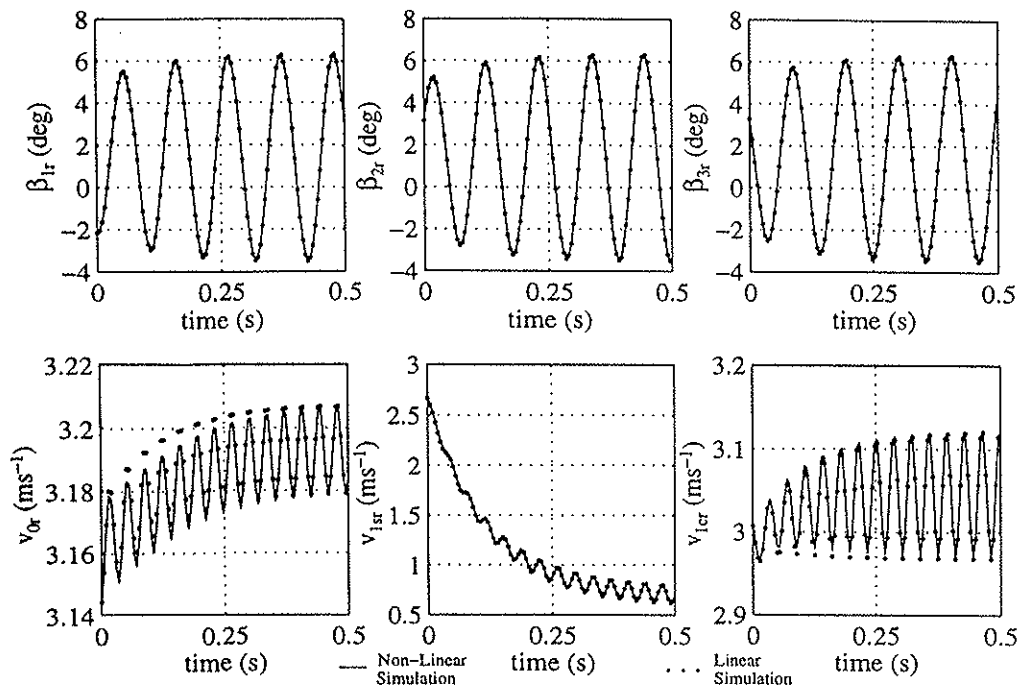


Figure 7: Comparison Between Responses Produced by Linear and Non-Linear Simulation Models For the Right Rotor States when Symmetric Disc Subsidence Mode ($\lambda=-8.6354$) is Injected onto Trimmed State Vector

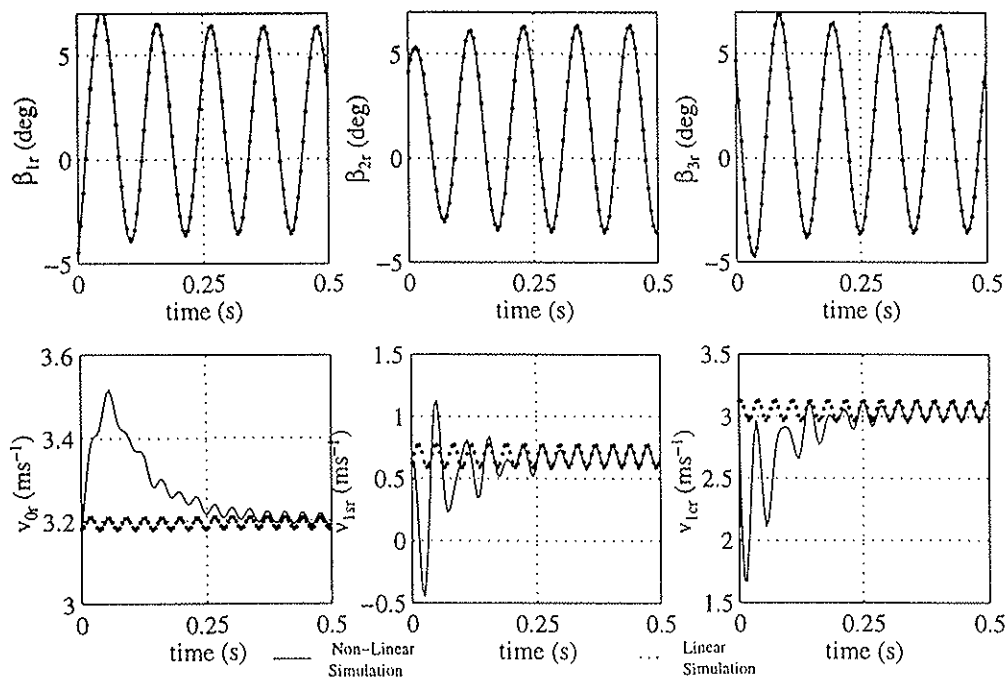


Figure 8: Comparison Between Responses Produced by Linear and Non-Linear Simulation Models For the Right Rotor States when Right Rotor Disc Progressing Mode ($\lambda=-13.8875 \pm 58.4953j$) is Injected onto Trimmed State Vector